Bioconjugate Chemistry

Article

Cite This: *Bioconjugate Chem.* 2019, 30, 1649−1657

pubs.acs.org/bc

Synthesis of the New Cyanine-Labeled Bacterial Lipooligosaccharides for Intracellular Imaging and in Vitro Microscopy Studies

Tung-Cheng Wang,[†] Florent Cochet,[‡] Fabio Alessandro Facchini,[‡] Lenny Zaffaroni,[‡] Christelle Serba,[§] Simon Pascal,[§] Chantal Andraud,[§] Andrea Sala,[§] Flaviana Di Lorenzo,[∥,⊥] Olivier Maury,[§] Thomas Huser,[†] and Francesco Peri*[,‡]

[†]Biomolecular Photonics, Department of Physics, University of Bielefeld. Universitätsstraße 25, 33615 Bielefeld, Germany

[‡]Department of Biotechnology and Biosciences, University of Milano-Bicocca. Piazza della Scienza, 2, 20126 Milano, Italy

[§]Laboratoire de Chimie, ENS de Lyon, 46 Allée d'Italie, 69364 Lyon Cedex 07, France

[∥]Department of Chemical Sciences, University of Naples, 80126, Naples, Italy

[⊥]Task Force on Microbiome Studies, University of Naples Federico II, 80126 Naples, Italy

Supporting Information

ABSTRACT: Endotoxin (lipooligosaccharide, LOS, and lipopolysaccharide, LPS) is the major molecular component of Gram-negative bacteria outer membrane, and very potent pro-inflammatory substance. Visualizing and tracking the distribution of the circulating endotoxin is one of the fundamental approaches to understand the molecular aspects of infection with subsequent inflammatory and immune responses, LPS also being a key player in the molecular dialogue between microbiota and host. While fluorescently labeled LPS has previously been used to track its subcellular localization and colocalization with TLR4 receptor and downstream effectors, our knowledge on lipopolysaccharide (LOS) localization and cellular activity remains almost unexplored. In this study, LOS was labeled with a novel fluorophore, Cy7N, featuring a large Stokes-shifted emission in the deep-red spectrum resulting in lower light scattering and better imaging contrast. The LOS-Cy7N chemical identity was determined by mass spectrometry, and immunoreactivity of the conjugate was evaluated. Interestingly, its application to microscopic imaging showed a faster cell internalization compared to LPS-Alexa488, despite that it is also CD14-dependent and undergoes the same endocytic pathway as LPS toward lysosomal detoxification. Our results suggest the use of the new infrared fluorophore Cy7N for cell imaging of labeled LOS by confocal fluorescence microscopy, and propose that LOS is imported in the cells by mechanisms different from those responsible for LPS uptake.

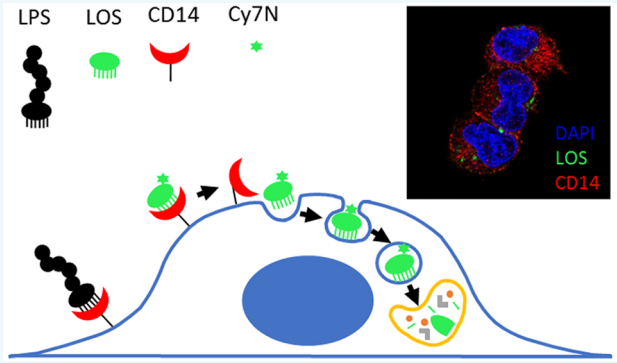

INTRODUCTION

Endotoxins (LPS and its truncated version LOS), also defined as pathogen-associated molecular patterns (PAMPs), are very toxic molecules released from the cell wall of Gram-negative bacteria and they are able to activate host inflammatory and immune responses at picomolar concentrations through the interaction with a specific pattern recognition receptor (PRR), the Toll-like Receptor 4 (TLR4). Severe sepsis and septic shock are life-threatening pathological diseases still lacking pharmacological treatment which derive from excessive TLR4 activation by circulating bacterial endotoxins.[1] Endotoxins and other PAMPs are also fundamental molecular players in the communication of gut microbiota with other organs and body districts, including the central nervous system.[2] LPS activation of endothelial TLR4 in the brain has recently been proposed as a model of pathogenesis for brain diseases, including cerebral cavernous malformations (CCMs) that are a cause of stroke and seizures.[2] In this model, bacteria in the gut are the source of LPS that enters the blood circulation, activates brain endothelial TLR4 receptors, and, in turn, drives intracellular signaling to induce the pathology. The ability to track endotoxins in the body can therefore provide important information about the molecular mechanisms by which intestinal microbial communities influence other organs and communicate with the brain, while the possibility to visualize TLR4-mediated LPS transport in cells can be used to clarify molecular mechanisms of TLR4 activation and signaling.

Received: January 17, 2019
Revised: May 24, 2019
Published: May 28, 2019

DOI: 10.1021/acs.bioconjchem.9b00044
Bioconjugate Chem. 2019, 30, 1649−1657

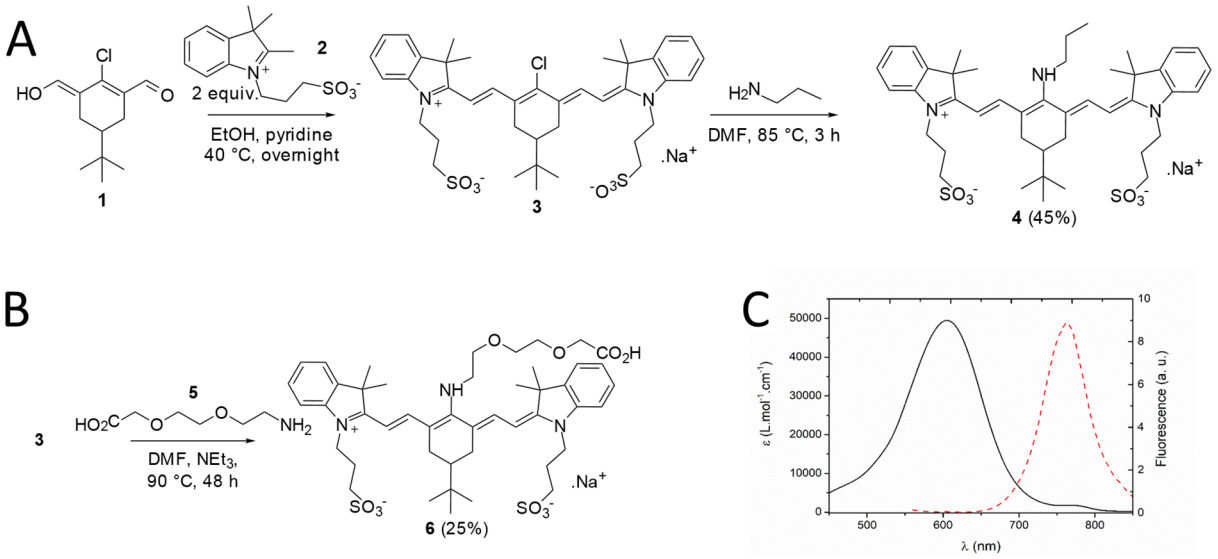

Figure 1. (A,B) Synthesis of the reference amino-heptamethine dye (Cy7N, **4**) and corresponding functionalized analogue (CDE-Cy7N, **6**; MW = 880.4). (C) Absorption (black, plain line) and fluorescence (red, dashed line) spectra of **4** in water. λ_{abs} = 605 nm; λ_{em} = 764 nm; ϕ_{fl} = 0.06.

LPS is transported to cell membranes by the sequential action of LPS-binding protein (LBP) and CD14. LBP acts to transfer LPS monomers out of LPS aggregates to a binding site on CD14; the LPS-CD14 complex then facilitates LPS transfer to TLR4-bound MD-2 adaptor and the formation of the activated homodimer $(TLR4/MD\text{-}2/LPS)_2$.[3] Ligand-induced formation of the TLR4/MD-2 homodimer on the plasma membrane of TLR4-HEK cells has recently been investigated using fluorescent protein-tagged TLR4 and quantitative single-molecule localization microscopy (SMLM).[4] Interestingly, 48% of fluorescent TLR4 molecules on the cell membrane were present as dimers even in the absence of LPS. The addition of *E. coli* LPS agonist induced the formation of 74% dimer, while the treatment with the antagonist *Rhodobacter sphaeroides* LPS gave 100% monomeric TLR4.

Once bound to MD-2 and associated with TLR4 into the homodimer, LPS initiates two independent signal pathways:[5,6] the MyD88-dependent pathway, which starts at the cell membrane with the formation of the Myddosome,[7] a macromolecular signaling complex formed by MyD88 and IRAK members leading to NF-κB activation and production of inflammatory cytokines. Alternatively, the TRIF-dependent pathway, which signals from the early endosomes, is activated and leads to the formation of the supramolecular Triffosome complex to drive type I interferon production and delayed NF-κB activation.[8]

Data using single molecule fluorescence (SMF) show that LPS stabilizes preformed TLR4/MD2 dimers to drive signaling;[4] however, other published studies suggest that, under certain circumstances, TLR4 clustering may take place.[9] While the majority of biophysical studies on LPS/TLR4 have used fluorescently labeled TLR4 to determine its location on the cell membrane, leading to eventual clustering and endocytosis of the TLR4/MD2 receptor complex, fluorescent LPS/LOS are fundamental molecular tools for investigating the body distribution and receptor-dependent cellular trafficking of bacterial endotoxin. Moreover, the conjugation of fluorescent agents reported so far were accomplished solely with LPS,[10−13] where the fluorophores were chemically attached to the hydroxyl groups of O-antigen, which is absent in LOS. Therefore, the labeling on LOS is still undocumented and should otherwise provide useful complementary information.

To this end, we decided to use cyanine-based fluorophores widely used in protein labeling for microscopic imaging[14] and in particular Cy7 derivatives known for their fluorescence in the near-infrared region (NIR), where they provide excellent contrast on biological samples. The cyanine fluorescent scaffold has already been used for a number of imaging applications including intracellular pH determination or ion sensing,[15−17] as contrast agent for surgery,[18] and for cancer detection and therapy.[19−21] However, Cy7 dyes suffer some inherent drawbacks, such as a very small Stokes-shift, which makes imaging experiments more difficult. Here, we explored the possibility to exploit the far-red fluorescence emission of the amino-heptamethine fluorophore (Cy7N), featuring a larger Stokes-shift (Δ = 3440 cm^{-1}), where the intense fluorescence of Cy7N is emitted in the far-red to NIR (λ_{em} = 764 nm) and consequently enables bioimaging experiments in the optically transparent spectral window where absorption and scattering of incident light are minimal.[22,23]

In the present study, Cy7N was functionalized with a carboxyl-diethylenglycolamine (CDE) linker to label LOS endotoxin through the reaction with a nucleophilic phosphoethanolamine group on LOS to obtain the fluorescently tagged LOS-Cy7N conjugate for *in vitro* microscopy studies. The use of Cy7N-labeled LOS enables us for the first time to explore its cell binding, internalization, and vesicle transport in single cells and compare it with fluorescent LPS.

RESULTS AND DISCUSSION

Synthesis of Conjugable CDE-Cy7N. The Cy7N fluorophores were designed by introducing sulfonate functions to optimize their solubility in biological media, while the rigidity of the heptamethine skeleton was ensured by a *tert*-butyl cyclohexenyl framework, limiting fluorescence losses by nonradiative deexcitation.[24] The synthesis of the reference amino-heptamethine Cy7N **4** (Figure 1A) and carboxyl-diethylenglycolamine (CDE)-functionalized Cy7N **6** (CDE-Cy7N, Figure 1B) was carried out using classical condi-

DOI: 10.1021/acs.bioconjchem.9b00044
Bioconjugate Chem. 2019, 30, 1649−1657

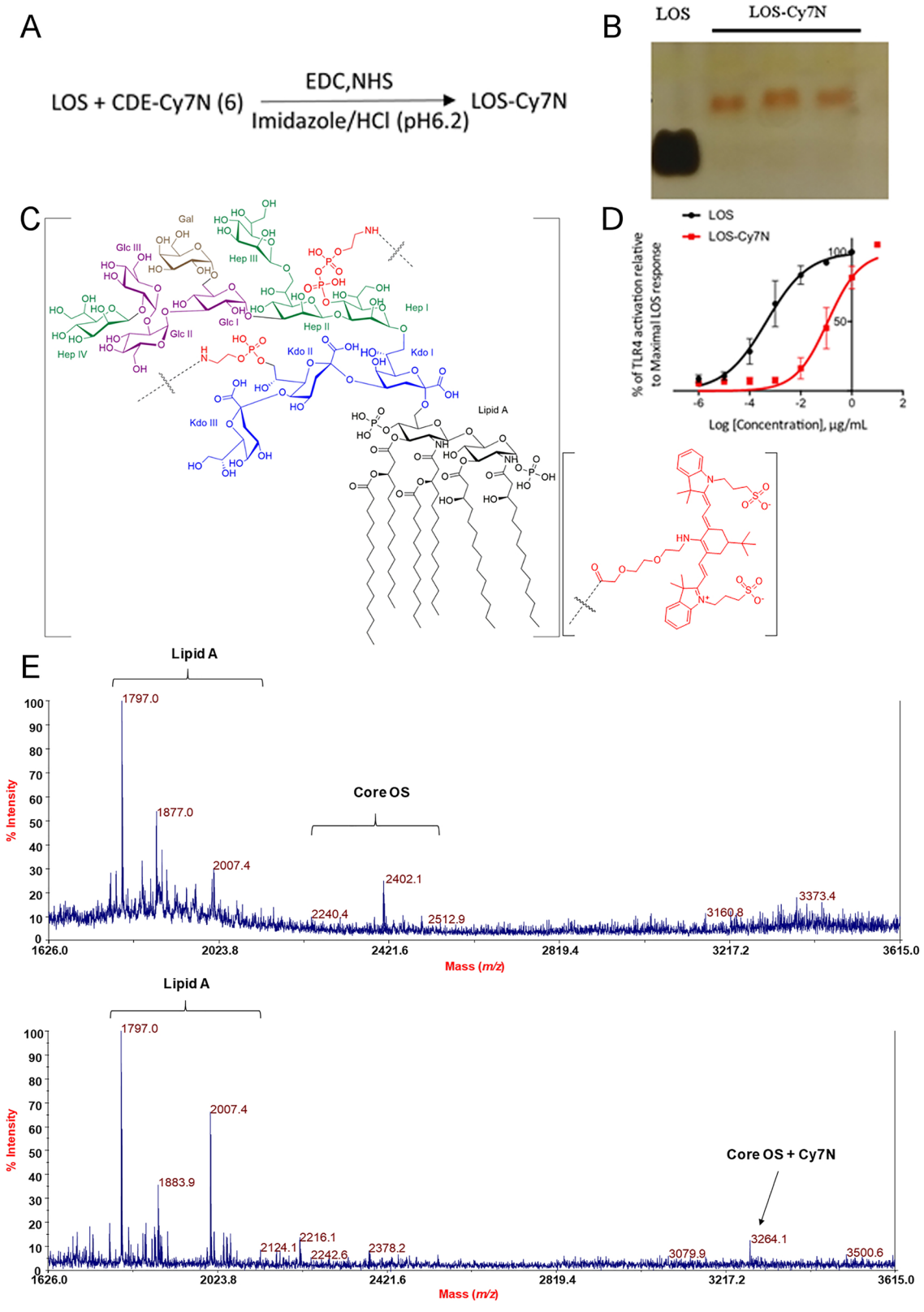

Figure 2. (A) Fluorescence labeling of *E. coli* LOS with CDE-Cy7N **6** give rise to LOS-Cy7N. (B) SDS-PAGE of three fractions recovered after two PD-10 columns is revealed by silver staining. (C) Chemical structure of LOS conjugated to one CDE-Cy7N unit attached to the monophosphoethanolamine of Kdo II or Hep I. (D) Bioactivities of LOS-Cy7N and native LOS were measured by TLR4-dependent SEAP reporter gene assay. Data points represent the mean of percentage ± SEM of at least three independent experiments. (E) Top: Zoom of the negative ion MALDI MS spectrum of the *E. coli* strain MG1655 showing the peaks relative to the lipid A and core OS species. Bottom: Zoom of the negative ion MALDI MS spectrum of the LOS-Cy7N showing the peaks relative to the lipid A species and to the core OS decorated by one Cy7N unit.

DOI: 10.1021/acs.bioconjchem.9b00044
Bioconjugate Chem. 2019, 30, 1649−1657

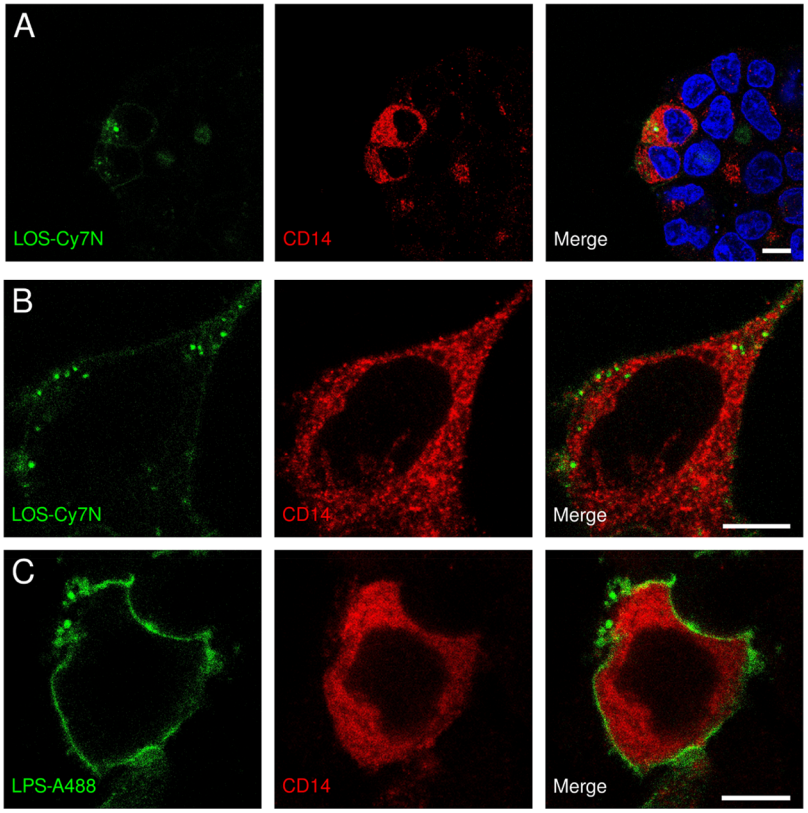

Figure 3. Specific binding of LOS-Cy7N and LPS-Alexa488 to CD14-transfected HEK-293T cells imaged by confocal fluorescence microscopy. (A) Cells were treated with LOS-Cy7N for 60 min, fixed, immunostained with anti-CD14 antibody, and counterstained with DAPI. Note that LOS-Cy7N is visualized on two CD14-expressing cells whereas it is absent in other cells revealed by DAPI staining of the nuclei. (B) Same treatment as in A, but with higher magnification on a single cell. The cell surface bound LOS-Cy7N is found rapidly internalized into the CD14-immunopositive cells as endosomal vesicles. (C) Cells treated with LPS-Alexa488 for the same incubation time showed fluorescence signal mostly resided on the plasma membrane and formed extracellular vesicles via possible exocytosis. Scale bar = 10 μm.

tions.[23,25] Briefly, the corresponding chloro-heptamethine precursor **3** was substituted in the presence of *n*-propylamine or 2-[2-(2-aminoethoxy)ethoxy]acetic acid **5** in DMF to afford dyes **4** and **6** as blue solids in 45% and 25% yields, respectively (Figure 1A and B). The photophysical properties of this type of cyanine dyes were investigated in the reference fluorophore Cy7N **4** and fluorescence spectra were recorded in water (Figure 1C). The chromophore presents a broad absorption band centered at 605 nm and an emission in the far-red range, characterized by a particularly large Stokes shift (ca. 3440 cm^{-1}). The fluorescence quantum yield is however noticeably decreased in water, as already reported for analogous polymethine derivatives.[24] Introduction of functional group on CDE-Cy7N **6** has no influence on the optical properties (Figure S1).[23,24,26] Cy7N was chosen for its particularly interesting photophysical properties,[14,27] such as featuring sulfonate side-chains that provide good solubility in aqueous media which is a critical parameter for imaging. Importantly, the central amino substitution confers optimal optical properties such as a significant Stokes shift and strong emission in the biologically transparent spectral window, which are highly beneficial to improve imaging contrast with the possibility to functionalize the central cyclohexene moiety with linkers containing terminal reactive groups for subsequent bioconjugation. Moreover, given that Cy7N can be excited similarly to Cy5 and it fluoresces with a larger Stokes shift, which trespasses beyond the typical Cy5 emission; it also permits a feasible approach to obtain two-color images of both cyanine dyes with a single excitation line (Figure S1). With these advantages taken together, we then applied the CDE-Cy7N **6** for conjugation to the endotoxin, LOS, to demonstrate its usefulness for fluorescence microscopy.

Bioconjugation of CDE-Cy7N to LOS. LOS (10 mg, 1 equiv) extracted and purified from *E. coli* strain MG1655, was dissolved in imidazole/HCl buffer (pH = 6.2). CDE-Cy7N **6** (5 equiv) was added together with the condensing agent 1-ethyl-3-(3-(dimethylamino)propyl) carbodiimide (EDC, 5 equiv), and a catalytic amount of the acyl-transfer catalyst *N*-hydroxysuccinimide (NHS) (Figure 2A). The mixture was stirred overnight at room temperature, then extracted with dichloromethane and the aqueous phase containing the conjugation product was purified by chromatography through 2 cycles of PD-10 column LOS-Cy7N. The purity of the conjugate was assessed by discontinuous SDS-PAGE (18% separating gel and 5% stacking gel) (Figure 2B and S2). The attachment of one CDE-Cy7N to LOS has been designed to be site-specific on the ethanolamine groups on KdoII or HepI phosphates (Figures 2C). The effective attachment of one CDE-Cy7N to core OS has been determined by MALDI mass spectrometry (MS) analysis of the LOS-Cy7N (Figure 2E, bottom) vs the underivatized *E. coli* LOS (Figure 2E, top). In both negative-ion MALDI MS spectra, the typical ion peaks originated from the cleavage of the labile glycosidic bond between Kdo and the lipid A moiety, yielding either core OS and lipid A ions, were clearly detectable. The observation in the spectrum of the LOS-Cy7N (Figure 2E, bottom), of the

DOI: 10.1021/acs.bioconjchem.9b00044
Bioconjugate Chem. 2019, 30, 1649−1657

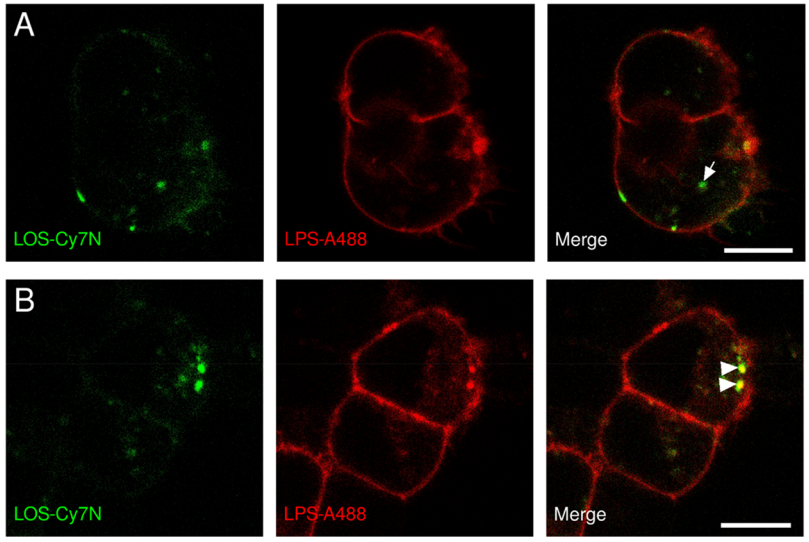

Figure 4. Confocal microscopic images of transfected HEK-293T cells cotreated with LOS-Cy7N and LPS-Alexa488 for 30 (A) and 120 min (B). (A) LOS-Cy7N appeared to be faster internalized in the absence of LPS-Alexa488 (arrow). (B) However, LPS-Alexa488 can be later found in cells with prolonged incubation and they, if not all, colocalized with LOS-Cy7N in vesicles just beneath the plasma membrane (arrowheads). Note that fluorescent ligands are not homogeneously distributed on cell surface, they instead appear as organized domain structures which are more pronounced for LOS-Cy7N. Scale bar = 10 μm.

peak at m/z 3264.1 matching with the *E. coli* strain MG1655 core OS built up of 3 Kdo, 4 Hep, 4 Hex, 1 PEtN, and 1 PPEtN (m/z 2402.1) plus 862 amu, namely decorated by one CDE-Cy7N unit, was crucial to verify the successful conjugation; finally, no peaks relative to underivatized core OS have been identified (Figure 2E, bottom).

Evaluation of LOS-Cy7N Bioactivity. The bioactivity of LOS-Cy7N in terms of its capacity to activate TLR4 was assayed on HEK-Blue hTLR4 reporter cells. This cell line provides stable expression of all proteins of the TLR4 receptor complex, namely, TLR4, MD-2, and membrane-bound CD14, and an inducible secreted embryonic alkaline phosphatase (SEAP) reporter gene placed under the control of transcription factors NF-κB and AP-1. The activation of TLR4/MD-2/LOS-Cy7N induces the activation of NF-κB and AP-1 leading to production and secretion of SEAP in the cell culture media. The levels of SEAP can easily be determined by incubating the enzyme with *para*-nitrophenyl phosphate (pNPP). Cells were treated with increasing concentrations of both fluorescently labeled LOS-Cy7N and unconjugated LOS (10^{-6} to 10^{1} μg/mL), and SEAP levels were quantified after 16 h of incubation (Figure 2D). Although the potency of LOS-Cy7N as TLR4 agonist is 3 orders of magnitude lower than LOS (EC_{50} of LOS-Cy7N and unconjugated LOS are 0.1 μg/mL and 0.45 ng/mL, respectively), Cy7N-labeled LOS activates TLR4 pathway in a comparable way than the unlabeled molecule at a concentration of 1 μg/mL. The results revealed that LOS-Cy7N was active for inducing TLR4 activation, though the addition of Cy7N fluorophore substantially reduced the immunogenicity compared to LOS. The cause is possibly due to the physical hindrance of the Cy7N labeling on the inner core of LOS where the interaction between TLR4 and LOS is partially masked and thus has negative impact on the ligand recognition and formation of the receptor complex.[28]

Cell Imaging of Cy7N-Labeled LOS. LOS-Cy7N was tracked in cells through confocal fluorescence microscopy. To observe the presence of LOS-Cy7N, we transiently expressed CD14 in HEK-293T cells because the introduction of CD14 in this cell type was required for cell binding of fluorescently labeled LPS[29,30] and also for the subsequent endocytosis that starts inflammatory cascade.[31,32] Within 1 h of incubation, the fluorescent signal of LOS-Cy7N was found in CD14-positive cells which were immunolabeled with the corresponding antibody, but not in the cells which did not express CD14 after transfection (Figure 3A). This observation strongly suggests that LOS retains its ability to bind CD14 after conjugation with cyanine and the internalization of the LOS-Cy7N is CD14-dependent. Other cyanine-labeled LPS, as LPS-Cy5,[29] probably behave similarly to LOS-Cy7N and CD14 binding is an important event leading to cell internalization. At the single cell level LOS-Cy7N was noticeably found on the plasma membrane, although primarily in the internalized vesicles (Figure 3B). This suggests that CD14 promotes the uptake of LOS-Cy7N into early endosomes.

For comparison to previously reported fluorescent ligands,[13] we used Alexa488-labeled LPS as a control, with which the cells were treated in the same conditions as LOS-Cy7N. Although the binding of LPS-Alexa488 was also found on the CD14-expressing cells, it was mainly localized at the cell surface, without entering into the cells (Figure 3C). On the contrary, LOS-Cy7N was readily taken up by the cells and internalized (Figure 3B). Ectopical expression of CD14 in HEK-293T cells proved to be essential for both surface binding and subsequent internalization of LOS-Cy7N, of which the nontransfected cells are not capable. We did not observe co-internalization of membrane-bound CD14 with LOS-Cy7N, most likely because CD14 was predominantly produced in the soluble form in the cytoplasm. We assume that only a limited amount of CD14 was linked to the glycosylphosphatidyl inositol (GPI) linker to be anchored to the plasma membrane, where its presence is overwhelmed by cytoplasmic CD14 and thus beyond the detection of a single optical section as seen by confocal microscopy. We hypothesize that it will be possible to visualize the membrane-bound CD14 (mCD14) by total internal reflection fluorescence microscopy by which its colocalization with fluorescent endotoxins can be clearly

DOI: 10.1021/acs.bioconjchem.9b00044
Bioconjugate Chem. 2019, 30, 1649−1657

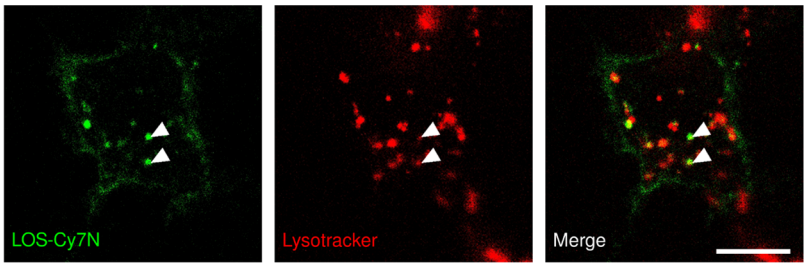

Figure 5. Subcellular localization study of endocytic vesicles of LOS-cy7N. Cells were first treated with LOS-Cy7N for 60 min, briefly washed with PBS, then incubated 5 min with lysotracker before imaging. The arrowheads depict the overlapped labeling. Scale bar = 10 nm.

determined. Interestingly, a similar study was conducted by introducing mCD14-EGFP to U373 cells, where its expression occurred predominantly at the cell surface. The authors found, however, that internalized BODIPY-LPS did not colocalize with mCD14-EGFP, suggesting that mCD14 did not accompany LPS during endocytic movement.[33] Such a phenomenon would likely depend on the specific cell types because LPS-induced CD14 internalization was previously shown in macrophages by flow cytometry.[32] However, the question whether mCD14, at least in imaging-based studies, is internalized together with the TLR4-LPS receptor complex or not, is still unanswered.

Nevertheless, we did observe a striking difference in the localizations between fluorescent LOS and LPS, indicating that LOS-Cy7N appears to be internalized faster than LPS-Alexa488 upon cell treatment. To directly compare the uptake events of the two fluorescent endotoxins, we then treated the cells with both fluorescent endotoxins and observed their interaction with the cells by time-lapsed imaging. Within a short period of incubation, LOS-Cy7N was partially translocated into the cells in contrast to the cell surface localization of LPS-Alexa488 (Figure 4A), which was then slowly internalized at later time points (Figure 4B). The cotreatment experiment thus indicated that while both fluorescent endotoxins followed the same steps toward cell internalization, the endocytosis of the LOS-Cy7N took place earlier than that of LPS-Alexa488. This may imply that different uptake mechanisms are used for each type of endotoxin molecules. The molecular mechanism of the CD14-mediated endocytic pathway is, however, less well understood: tyrosine kinase Syk and PLCγ2 are involved as downsteam effectors for LPS-induced endocytosis of TLR4.[32] Both clathrin and dynamin were proposed for the formation of LPS-internalized vesicles.[30,34] It remains to be discovered if the above-mentioned mechanisms also apply for LOS or if other molecular events facilitate the internalization of LOS faster than LPS.

Interestingly, the formation of internalized endotoxins in early endosomes provides a second signaling source other than the MyD88-dependent pathway, initiated by the assembly of adaptors TRAM and TRIF.[35,36] These adaptors mediate the activation of the transcription factor interferon regulatory factor-3 (IRF3), which regulates type I interferon (IFN) expression.[6] Since the LOS-Cy7N could be detected intracellularly, while LPS remained in the plasma membrane, the timing of signal triggers may result in different cell responses upon stimuli. For instance, LOS-induced cytotoxicity may largely rely on endosomal signaling rather than MyD88-dependent signaling and thus promotes different cell reactions from the cell surface-bound LPS in the first phase of cell activation (Figure S3). In fact, different modes of actions taken between two types of endotoxins have shown that the LOS can activate inflammasomes in dendritic cells in the absence of other accessories which are otherwise required for LPS.[37]

Finally, we are also interested in understanding the vesicle transport of internalized LOS-Cy7N. It is known that once LPS is internalized it undergoes the endocytic pathway to be processed and degraded in lysosomes, and this step is important for signal termination.[30] To see if LOS-Cy7N follows the same route, cells were treated with LOS-Cy7N and LysoTracker Green (Figure 5). Here, we also identified that a subset of the endocytosed LOS-Cy7N was indeed colocalized with lysosomal marker, which indicates that they were sorted to lysosomes for detoxification.

CONCLUSIONS

This is the first imaging study that shows how LOS interacts with cells (through receptors) and its distribution after cell uptake. To visualize the actions of LOS on treated cells, a new near-infrared fluorophore (Cy7N) was synthesized and its carboxylic acid derivative was successfully conjugated to one amino group of LOS extracted from a unique strain of *E. coli*. Contrary to commercially available fluorescent LPS, the fluorescently labeled endotoxin LOS-Cy7N was purified by chromatography with a high level of chemical purity.

The use of Cy7N as a fluorescent tag to follow spatially and temporally LOS cellular localization was proved by live-cell confocal microscopy imaging. The CD14 coreceptor is well-known as an important player in both endotoxin presentation to TLR4/MD-2 and in the internalization of the homodimeric $(TLR4/MD\text{-}2/ligand)_2$ complex. In particular, CD14 is required to visualize cell binding and the internalization of the fluorescent ligands. Here we have shown that LOS(-Cy7N) undergoes CD14-mediated endocytosis much faster than LPS(-Alexa488) upon cell surface binding, which indicates that the underlying uptake mechanisms of LOS may differ from those of LPS.

The LOS-Cy7N physicochemical properties (solubility) and optical parameters turned out to be optimal for the microscopy of biological media. The use of this LOS conjugate as a tagging tool for in vivo imaging can be envisaged, especially for studying the role of endotoxin in the dialogue between gut microbiota and other body districts and organs.

EXPERIMENTAL PROCEDURES

Synthesis. NMR spectra (^1H) were recorded on a Bruker Advance operating at 500.10. Data are listed in parts per million (ppm) and are reported relative to residual solvent peaks being used as internal standard. High resolution mass spectrometry measurements were performed at Centre

DOI: 10.1021/acs.bioconjchem.9b00044
Bioconjugate Chem. 2019, 30, 1649−1657

Commun de Spectrometrie de Masse (Villeurbanne, France). Starting materials were purchased from Sigma-Aldrich, Acros Organics, or Alfa Aesar with the best available quality grade. All reactions were routinely performed under argon atmosphere in anhydrous solvents. Column chromatography were performed using Acros Organics (0.035−0.070 mm) silica gel or neutral aluminum oxide (50−200 μm, 60 A). Compounds **1**,[38] **2**,[39] **3**,[25] and **4**[25] were prepared following previously reported protocols. **5** is simply prepared from the commercially available Fmoc-protected compound.

Compound 6. 100 mg of 3 (0.12 mmol, 1 equiv) and 59 mg of 5 (0.36 mmol, 3 equiv) were dissolved in 3 mL of anhydrous DMF and 150 μL of Et_3N (9 equiv) were added. The mixture was stirred at 80 °C for 2 days in the dark. After the solution was cooled down to room temperature, the solvent was evaporated under reduced pressure. The crude was dissolved in 1 mL of brine, and 2 mL of H_2O and was purified on automatic column (reverse phase bonded silica, C18-HP, 30 μm). The elution started with a mixture of H_2O:MeCN (90:10) and ended with 100% MeCN. After evaporation of the MeCN, water was removed by lyophilization overnight to afford the product as a blue solid in a 25% yield (26 mg).

^{1}H NMR (CD_3OD, 300 MHz, 25 °C): δ 7.82 (d, ^3J = 13 Hz, 2H), 7.38 (d, ^3J = 7 Hz, 2H), 7.30 (t, ^3J = 7 Hz, 2H), 7.18 (d, ^3J = 8 Hz, 2H), 7.08 (t, ^3J = 7 Hz, 2H), 5.99 (d, ^3J = 13 Hz, 2H), 4.17 (t, ^3J = 7 Hz, 4H), 4.12 (s, 2H), 3.93 (t, 2H), 3.79 (t, 2H), 3.78 (s, 2H), 2.93 (t, ^3J = 6 Hz, 4H), 2.82 (m, 2H), 2.20 (q, ^3J = 6 Hz, 4H), 2.03 (t, ^3J = 13 Hz, 2H), 1.70 (s, 6H), 1.69 (s, 6H), 1.31 (m, 1H), 1.09 (s, 9H). ^{13}C NMR (CD_3OD, 125.75 MHz, 25 °C): 172.8, 168.0, 143.0, 140.0, 139.7, 128.1, 122.6, 121.7, 108.8, 94.5, 70.3, 69.9, 68.0, 66.4, 49.6, 44.8, 44.3, 41.5, 39.1, 32.3, 27.8, 27.7, 26.3, 26.2, 23.2, 22.1. HRMS (ESI$^-$): $[M]^-$ = 880.3845 (calc. for $C_{46}H_{62}N_3O_{10}S_2$: 880.3882). UV−vis (CH_3OH): λ_{max} = 630 nm (ε_{max} = 76 500 L.mol^{-1}.cm^{-1}).

Absorption and Fluorescence. UV−vis-NIR absorption spectra were recorded on a Jasco V-670 spectrophotometer in spectrophotometric grade solvents (ca. 10^{-5} mol L^{-1}). Molar extinction coefficients (ε) were precisely determined at least two times. The luminescence spectra were measured using a Horiba-Jobin Yvon Fluorolog-3 Spectro fluorimeter, equipped with a three slit double grating excitation and emission monochromator with dispersions of 2.1 nm/mm (1200 grooves/mm). The steady-state luminescence was excited by unpolarized light from a 450 W xenon CW lamp and detected at an angle of 90° for diluted solution measurements (10 mm quartz cuvette) by a red-sensitive Hamamatsu R928 photomultiplier tube. Spectra were reference corrected for both the excitation source light intensity variation (lamp and grating) and the emission spectral response (detector and grating). Fluorescence quantum yields Q were measured in diluted solution with an optical density lower than 0.1 using the following equation $Q_x/Q_r = [A_r(\lambda)/A_x(\lambda)][n_x^2/n_r^2][D_x/D_r]$ were A is the absorbance at the excitation wavelength (λ), n the refractive index, and D the integrated intensity. "r" and "x" stand for reference and sample. Excitation of reference and sample compounds was performed at the same wavelength. Cresyl violet was used as reference (ϕ_{fl} = 0.55 in MeOH).

LOS Extraction and Purification. For lipooligosaccharide (LOS) extraction, *E. coli* strain MG1655 was grown at 37 °C in LD for 16 h. Culture was aseptically diluted 1:100 in fresh medium and grown until mid logarithmic phase (OD_{600} = 0.7−0.8). Cells were harvested by centrifugation (5000 × g, 20 min), washed in 50 mM NaH_2PO_4 pH 8.0 and cell pellets were stored at −20 °C before extraction. LOS was selectively extracted from dry cell pellets using phenol chloroform−light petroleum (PCP) procedure.[40] Briefly, a solution of aqueous 90% phenol chloroform−light petroleum (2:5:8 v/v/v), to which solid phenol was added until limpidness, was prepared. Dry cell pellets were suspended in PCP solutions (2.5%, w/v), stirred for 30 min, and extracted three times. Then, the light solvents were removed under vacuum and LOS was precipitated from the remaining phenol solution by adding water. The solid was centrifuged, collected, suspended in water, and dialyzed (cutoff 1000 Da) against distilled water for 3 days. Finally, it was lyophilized, and pure LOS was recovered. The yield of recovery from 1 g of *E. coli* used for extraction is typically in the range of 30−40 mg of dry LOS. Samples obtained from this procedure was analyzed by discontinuous SDS-PAGE (Sodium Dodecyl Sulfate Polyacrylamide Electrophoresis). The gel was prepared with 15% separating gel and 5% stacking gel. The gel was stained according to the silver stain procedure for lipopolysaccharide.[41]

MALDI MS of *E. coli* Strain MG1655 LOS and LOS-Cy7N. MALDI MS of intact LOS and conjugated LOS were recorded in reflectron mode and negative ion on an ABSCIEX TOF/TOF 5800 Applied Biosystems mass spectrometer, equipped with an Nd:YLF laser (λ = 345 nm), with a pulse length of <500 ps and a repetition rate of up to 1000 Hz. MALDI preparations were performed as previously reported.[42]

HEK-Blue hTLR4 Cells. HEK-Blue hTLR4 cells (InvivoGen) were cultured according to manufacturer's instructions. Briefly, cells were cultured (37 °C, 5% CO_2, 95% humidity) in DMEM high glucose medium supplemented with 10% fetal bovine serum (FBS), 2 mM glutamine, antibiotics, and 1× HEK-Blue Selection (InvivoGen). Cells were treated with the indicated concentrations of LOS-Cy7N and unconjugated LOS and incubated for 16 h. Supernatants were collected and SEAP levels were quantified by pNPP assay as indicator of TLR4 activation. Data were normalized compared to maximal TLR4 activation obtained by stimulating cells with 1 μg/mL LOS. Concentration-dependent data were fitted to a sigmoidal four-parameter logistic equation to determine EC_{50} values.

Confocal Microscopy. HEK-293T cells and hCD14 plasmid were gifts of Dr. Roman Jerala (Chemistry Institute, Slovenia). Cells were seeded in glass-bottom imaging chambers (ibidi), transfected with plasmids in a mixture of polyethylenimine. After 48 h post transfection, cells were treated with 1 μg/mL of Alexa Fluor 488-LPS (ThermoFischer, L23351) or LOS-Cy7N for indicated time, briefly washed with PBS before imaging. For immunofluorescence, cells were first fixed with 4% paraformaldehyde, permeabilized with 0.1% Triton X-100, blocked with 3% (w/v) BSA, followed by immunostaining with anti-CD14 antibody (Novus Biologicals, clone:4B4F12, 1:200) and secondary antibody conjugated to Alexa568 (ThermoFischer, 1:1000). Lysosomes were stained with 50 nM LysoTracker Green (ThermoFischer, L7526) according to manufacturer's instructions. Cell images were acquired on a Leica TCS SP8 microscope (Mannheim, Germany) using a 60×/1.2 NA water objective. Fluorescent labels were sequentially imaged by selecting individual excitation lines from a supercontinuum laser source. Controls were conducted to make sure images are free of crosstalk.

DOI: 10.1021/acs.bioconjchem.9b00044
Bioconjugate Chem. 2019, 30, 1649−1657

■ ASSOCIATED CONTENT

Supporting Information

The Supporting Information is available free of charge on the ACS Publications website at DOI: 10.1021/acs.bioconjchem.9b00044.

Further information on CDE-Cy7N spectra measured by fluorometer, schematic drawing of LOS-Cy7N and cell signaling of LPS/LOS (PDF)

■ AUTHOR INFORMATION

Corresponding Author

*E-mail: francesco.peri@unimib.it. Phone: +39.02.64483453.

ORCID

Fabio Alessandro Facchini: 0000-0002-4339-5845
Simon Pascal: 0000-0001-8387-494X
Olivier Maury: 0000-0002-4639-643X
Thomas Huser: 0000-0003-2348-7416
Francesco Peri: 0000-0002-3417-8224

Notes

The authors declare no competing financial interest.

■ ACKNOWLEDGMENTS

We thank Dr. Mojca Bencina and Ha Van Thai for technical assistance. This work is supported by funding from the European Union's Horizon 2020 research and innovation program under the Marie Sklodowska-Curie Grant Agreement No. 642157, project "TOLLerant" (www.tollerant.eu).

■ REFERENCES

(1) Whitfield, C., and Trent, M. S. (2014) Biosynthesis and export of bacterial lipopolysaccharides. *Annu. Rev. Biochem. 83*, 99−128.

(2) Tang, A. T., Choi, J. P., Kotzin, J. J., Yang, Y., Hong, C. C., Hobson, N., Girard, R., Zeineddine, H. A., Lightle, R., Moore, T., et al. (2017) Endothelial TLR4 and the microbiome drive cerebral cavernous malformations. *Nature 545*, 305−310.

(3) Ryu, J.-K., Kim, S. J., Rah, S.-H., Kang, J. I., Jung, H. E., Lee, D., Lee, H. K., Lee, J.-O., Park, B. S., Yoon, T.-Y., et al. (2017) Reconstruction of LPS Transfer Cascade Reveals Structural Determinants within LBP, CD14, and TLR4-MD2 for Efficient LPS Recognition and Transfer. *Immunity 46*, 38−50.

(4) Krüger, C. L., Zeuner, M.-T., Cottrell, G. S., Widera, D., and Heilemann, M. (2017) Quantitative single-molecule imaging of TLR4 reveals ligand-specific receptor dimerization. *Sci. Signaling 10*, eaan1308.

(5) Rosadini, C. V., and Kagan, J. C. (2017) Early innate immune responses to bacterial LPS. *Curr. Opin. Immunol. 44*, 14−19.

(6) Akira, S., and Takeda, K. (2004) Toll-like receptor signalling. *Nat. Rev. Immunol. 4*, 499−511.

(7) Lin, S.-C., Lo, Y.-C., and Wu, H. (2010) Helical assembly in the MyD88-IRAK4-IRAK2 complex in TLR/IL-1R signalling. *Nature 465*, 885−890.

(8) Tan, Y., and Kagan, J. C. (2017) Microbe-inducible trafficking pathways that control Toll-like receptor signaling. *Traffic 18*, 6−17.

(9) Motshwene, P. G., Moncrieffe, M. C., Grossmann, J. G., Kao, C., Ayaluru, M., Sandercock, A. M., Robinson, C. V., Latz, E., and Gay, N. J. (2009) An oligomeric signaling platform formed by the Toll-like receptor signal transducers MyD88 and IRAK-4. *J. Biol. Chem. 284*, 25404−25411.

(10) Troelstra, A., Antal-Szalmas, P., Graaf-Miltenburg, L., Weersink, A., Verhoef, J., van Kessel, K., and Van Strijp (1997) Saturable CD14-dependent binding of fluorescein-labeled lipopolysaccharide to human monocytes. *Infect. Immun. 65*, 2272−2277.

(11) Duheron, V., Moreau, M., Collin, B., Sali, W., Bernhard, C., Goze, C., Gautier, T., Pais de Barros, J.-P., Deckert, V., Brunotte, F., et al. (2014) Dual labeling of lipopolysaccharides for SPECT-CT imaging and fluorescence microscopy. *ACS Chem. Biol. 9*, 656−662.

(12) Thieblemont, N., Thieringer, R., and Wright, S. D. (1998) Innate Immune Recognition of Bacterial Lipopolysaccharide: Dependence on Interactions with Membrane Lipids and Endocytic Movement. *Immunity 8*, 771−777.

(13) Triantafilou, K., Triantafilou, M., and Fernandez, N. (2000) Lipopolysaccharide (LPS) labeled with Alexa 488 hydrazide as a novel probe for LPS binding studies. *Cytometry 41*, 316−320.

(14) Yuan, L., Lin, W., Zheng, K., He, L., and Huang, W. (2013) Far-red to near infrared analyte-responsive fluorescent probes based on organic fluorophore platforms for fluorescence imaging. *Chem. Soc. Rev. 42*, 622−661.

(15) Guo, Z., Kim, G.-H., Yoon, J., and Shin, I. (2014) Synthesis of a highly Zn(2+)-selective cyanine-based probe and its use for tracing endogenous zinc ions in cells and organisms. *Nat. Protoc. 9*, 1245−1254.

(16) Sun, C., Wang, P., Li, L., Zhou, G., Zong, X., Hu, B., Zhang, R., Cai, J., Chen, J., and Ji, M. (2014) A new near-infrared neutral pH fluorescent probe for monitoring minor pH changes and its application in imaging of HepG2 cells. *Appl. Biochem. Biotechnol. 172*, 1036−1044.

(17) Zhu, M., Shi, C., Xu, X., Guo, Z., and Zhu, W. (2016) Near-infrared cyanine-based sensor for Fe 3+ with high sensitivity: its intracellular imaging application in colorectal cancer cells. *RSC Adv. 6*, 100759−100764.

(18) Njiojob, C. N., Owens, E. A., Narayana, L., Hyun, H., Choi, H. S., and Henary, M. (2015) Tailored near-infrared contrast agents for image guided surgery. *J. Med. Chem. 58*, 2845−2854.

(19) Meng, X., Yang, Y., Zhou, L., Zhang, L., Lv, Y., Li, S., Wu, Y., Zheng, M., Li, W., Gao, G., et al. (2017) Dual-responsive molecular probe for tumor targeted imaging and photodynamic therapy. *Theranostics 7*, 1781−1794.

(20) Shen, Z., Prasai, B., Nakamura, Y., Kobayashi, H., Jackson, M. S., and McCarley, R. L. (2017) A near-infrared, wavelength-shiftable, turn-on fluorescent probe for the detection and imaging of cancer tumor cells. *ACS Chem. Biol. 12*, 1121−1132.

(21) Yen, S. K., Jańczewski, D., Lakshmi, J. L., Dolmanan, S. B., Tripathy, S., Ho, V. H. B., Vijayaragavan, V., Hariharan, A., Padmanabhan, P., Bhakoo, K. K., et al. (2013) Design and synthesis of polymer-functionalized NIR fluorescent dyes–magnetic nanoparticles for bioimaging. *ACS Nano 7*, 6796−6805.

(22) Frangioni, J. (2003) In vivo near-infrared fluorescence imaging. *Curr. Opin. Chem. Biol. 7*, 626−634.

(23) Peng, X., Song, F., Lu, E., Wang, Y., Zhou, W., Fan, J., and Gao, Y. (2005) Heptamethine cyanine dyes with a large stokes shift and strong fluorescence: a paradigm for excited-state intramolecular charge transfer. *J. Am. Chem. Soc. 127*, 4170−4171.

(24) Pascal, S., Denis-Quanquin, S., Appaix, F., Duperray, A., Grichine, A., Le Guennic, B., Jacquemin, D., Cuny, J., Chi, S.-H., Perry, J. W., et al. (2017) Keto-polymethines: a versatile class of dyes with outstanding spectroscopic properties for in cellulo and in vivo two-photon microscopy imaging. *Chem. Sci. 8*, 381−394.

(25) Pascal, S., Haefele, A., Monnereau, C., Charaf-Eddin, A., Jacquemin, D., Le Guennic, B., Andraud, C., and Maury, O. (2014) Expanding the polymethine paradigm: evidence for the contribution of a bis-dipolar electronic structure. *J. Phys. Chem. A 118*, 4038−4047.

(26) Grichine, A., Haefele, A., Pascal, S., Duperray, A., Michel, R., Andraud, C., and Maury, O. (2014) Millisecond lifetime imaging with a europium complex using a commercial confocal microscope under one or two-photon excitation. *Chem. Sci. 5*, 3475−3485.

(27) Guo, Z., Park, S., Yoon, J., and Shin, I. (2014) Recent progress in the development of near-infrared fluorescent probes for bioimaging applications. *Chem. Soc. Rev. 43*, 16−29.

(28) Park, B. S., Song, D. H., Kim, H. M., Choi, B.-S., Lee, H., and Lee, J.-O. (2009) The structural basis of lipopolysaccharide recognition by the TLR4-MD-2 complex. *Nature 458*, 1191−1195.

(29) Latz, E., Visintin, A., Lien, E., Fitzgerald, K. A., Monks, B. G., Kurt-Jones, E. A., Golenbock, D. T., and Espevik, T. (2002)

DOI: 10.1021/acs.bioconjchem.9b00044
Bioconjugate Chem. 2019, 30, 1649−1657

Lipopolysaccharide rapidly traffics to and from the Golgi apparatus with the toll-like receptor 4-MD-2-CD14 complex in a process that is distinct from the initiation of signal transduction. *J. Biol. Chem. 277*, 47834−47843.
(30) Husebye, H., Halaas, Ø., Stenmark, H., Tunheim, G., Sandanger, Ø., Bogen, B., Brech, A., Latz, E., and Espevik, T. (2006) Endocytic pathways regulate Toll-like receptor 4 signaling and link innate and adaptive immunity. *EMBO J. 25*, 683−692.
(31) Zanoni, I., Ostuni, R., Marek, L. R., Barresi, S., Barbalat, R., Barton, G. M., Granucci, F., and Kagan, J. C. (2011) CD14 controls the LPS-induced endocytosis of Toll-like receptor 4. *Cell 147*, 868−880.
(32) Tan, Y., Zanoni, I., Cullen, T. W., Goodman, A. L., and Kagan, J. C. (2015) Mechanisms of Toll-like Receptor 4 Endocytosis Reveal a Common Immune-Evasion Strategy Used by Pathogenic and Commensal Bacteria. *Immunity 43*, 909−922.
(33) Vasselon, T., Hailman, E., Thieringer, R., and Detmers, P. A. (1999) Internalization of Monomeric Lipopolysaccharide Occurs after Transfer out of Cell Surface CD14. *J. Exp. Med. 190*, 509−521.
(34) Klein, D. C. G., Skjesol, A., Kers-Rebel, E. D., Sherstova, T., Sporsheim, B., Egeberg, K. W., Stokke, B. T., Espevik, T., and Husebye, H. (2015) CD14, TLR4 and TRAM Show Different Trafficking Dynamics During LPS Stimulation. *Traffic 16*, 677−690.
(35) Kagan, J. C., Su, T., Horng, T., Chow, A., Akira, S., and Medzhitov, R. (2008) TRAM couples endocytosis of Toll-like receptor 4 to the induction of interferon-beta. *Nat. Immunol. 9*, 361−368.
(36) Tanimura, N., Saitoh, S., Matsumoto, F., Akashi-Takamura, S., and Miyake, K. (2008) Roles for LPS-dependent interaction and relocation of TLR4 and TRAM in TRIF-signaling. *Biochem. Biophys. Res. Commun. 368*, 94−99.
(37) Zanoni, I., Bodio, C., Broggi, A., Ostuni, R., Caccia, M., Collini, M., Venkatesh, A., Spreafico, R., Capuano, G., and Granucci, F. (2012) Similarities and differences of innate immune responses elicited by smooth and rough LPS. *Immunol. Lett. 142*, 41−47.
(38) Reynolds, G. A., and Drexhage, K. H. (1977) Stable heptamethine pyrylium dyes that absorb in the infrared. *J. Org. Chem. 42*, 885−888.
(39) Flanagan, J. H., Khan, S. H., Menchen, S., Soper, S. A., and Hammer, R. P. (1997) Functionalized tricarbocyanine dyes as near-infrared fluorescent probes for biomolecules. *Bioconjugate Chem. 8*, 751−756.
(40) Galanos, C., Luderitz, O., and Westphal, O. (1969) A New Method for the Extraction of R Lipopolysaccharides. *Eur. J. Biochem. 9*, 245−249.
(41) Kittelberger, R., and Hilbink, F. (1993) Sensitive silver-staining detection of bacterial lipopolysaccharides in polyacrylamide gels. *J. Biochem. Biophys. Methods 26*, 81−86.
(42) Di Lorenzo, F., Sturiale, L., Palmigiano, A., Lembo-Fazio, L., Paciello, I., Coutinho, C. P., Sá-Correia, I., Bernardini, M., Lanzetta, R., Garozzo, D., Silipo, A., and Molinaro, A. (2013) Chemistry and biology of the potent endotoxin from a Burkholderia dolosa clinical isolate from a cystic fibrosis patient. *ChemBioChem 14* (9), 1105−1115.

DOI: 10.1021/acs.bioconjchem.9b00044
Bioconjugate Chem. 2019, 30, 1649−1657